

Data-Driven Terramechanics Approach Towards a Realistic Real-Time Simulator for Lunar Rovers

Jakob M. Kern, James M. Hurrell, Shreya Santra, Keisuke Takehana, Kentaro Uno, and Kazuya Yoshida

Abstract—High-fidelity simulators for the lunar surface provide a digital environment for extensive testing of rover operations and mission planning. However, current simulators focus on either visual realism or physical accuracy, which limits their capability to replicate lunar conditions comprehensively. This work addresses that gap by combining high visual fidelity with realistic terrain interaction for a realistic representation of rovers on the lunar surface. Because direct simulation of wheel-soil interactions is computationally expensive, a data-driven approach was adopted, using regression models for slip and sinkage from data collected in both full-rover and single-wheel experiments and simulations. The resulting regression-based terramechanics model accurately reproduced steady-state and dynamic slip, as well as sinkage behavior, on flat terrain and slopes up to 20° , with validation against field test results. Additionally, improvements were made to enhance the realism of terrain deformation and wheel trace visualization. This method supports real-time applications that require physically plausible terrain response alongside high visual fidelity.

I. INTRODUCTION

The limited opportunities for testing lunar rovers during real missions highlight the need for realistic lunar surface simulators. A digital environment allows for replicating lunar conditions, ranging from visual features, such as extreme lighting with long shadows, to terrain features. However, for planetary rover operations and mission planning, it is essential that the simulated lunar environment not only appears visually realistic but also accurately models the physical interaction between the rover and the terrain. Especially, the slip ratio, a measure of wheel traction, and wheel sinkage into the terrain are critical features that occur on granular soil, such as the lunar regolith. While the wheel-soil interaction can be analyzed in detail using contact dynamics and particle simulations, this approach is computationally intensive and not suitable for real-time applications.

To address this limitation, this study employs a data-driven approach to enhance the physical fidelity of wheel-terrain interactions for real-time lunar surface simulations, as shown in Fig. 1. Regression models for slip ratio and sinkage were derived from experiments conducted with a high-speed rover [1] at the Space Exploration Field in the Japan Aerospace Exploration Agency (JAXA) Sagamihara

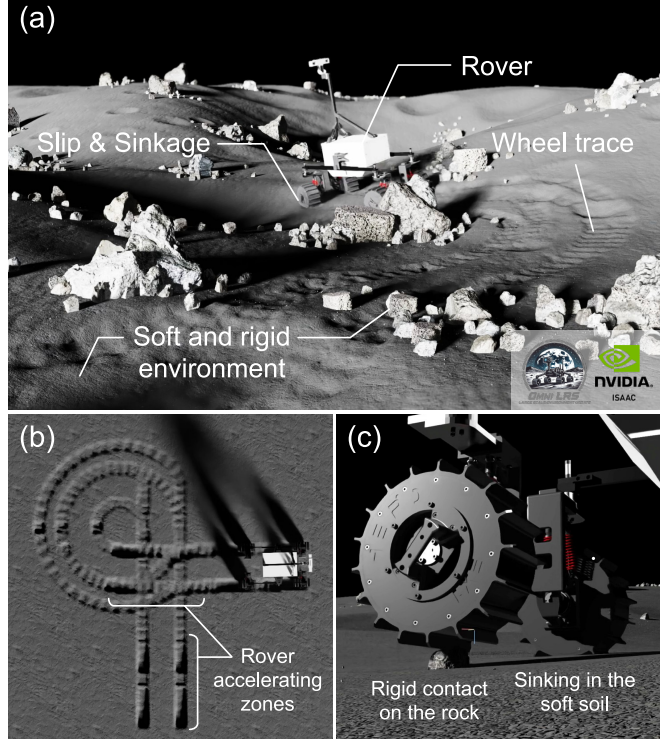


Fig. 1. (a) Data-driven terramechanics model for recreating realistic wheel slip, sinkage and wheel traces inside the real-time lunar surface simulator OmniLRS. (b) A rover makes physically reasonable wheel traces in our simulator. (c) Rigid and soft contacts are treated respectively.

Campus [2]. These models were integrated into a rigid-body simulation framework to replicate realistic wheel slip and sinkage in a digital environment while maintaining low computational costs. The main contributions of this work are:

- Wheel slip implementation, based on wheel velocity and slope angle
- Wheel sinkage implementation, based on slip ratio and wheel load
- Terrain deformation, based on slip ratio, to improve the realism of rover wheel traces

This work is integrated into the open-source OmniLRS simulator [3], which is based on NVIDIA IsaacSim [4], and extends its capabilities for planetary rover testing with improved physics fidelity.

II. RELATED WORKS

High-fidelity simulation of lunar rover mobility requires both visually convincing environments and physically ac-

*This work was supported by JST Moonshot R&D Program, Grant Number JPMJMS223B.

All authors are with the Space Robotics Lab (SRL) in the Department of Aerospace Engineering, Graduate School of Engineering, Tohoku University, Sendai 980-8579, Japan.

The corresponding author is Jakob M. Kern.

(E-mail: kern.jakob.marian.s4@dc.tohoku.ac.jp)

curate wheel-soil interactions. However, existing simulation tools tend to prioritize one at the expense of the other. Real-time lunar surface simulators typically emphasize high visual fidelity and integration with robotic control frameworks, but they often simplify terrain interactions. On the other hand, high-fidelity terramechanics simulators model granular soil dynamics in detail but are too computationally intensive for real-time use. In this section, we review key works from both areas and motivate our approach, which bridges the gap between them.

A. Real-time Lunar Surface Simulators

Several high-fidelity lunar surface simulators for real-time applications are actively being developed, with a primary focus on visual realism. The lunar environments use rigid terrain models and simple physics models, limiting their utility for realistic rover mobility simulation.

One example is the **Digital Lunar Exploration Sites (DLES)** [5], [6] developed by NASA's Johnson Space Center, which provides a detailed model of the lunar South Pole, derived from the Lunar Orbiter Laser Altimeter (LOLA) [7]. The authors describe the processing of digital elevation maps and the efficient handling of large-scale environments, including craters and boulders. While DLES was designed for use across multiple rendering engines, the **DLES Unreal Simulation Tool (DUST)** [8] integrates the DLES terrain database into Unreal Engine 5. It features high-resolution terrain, realistic lighting, and tools for planning rover traverses. However, it lacks terrain deformation modeling and complex wheel-terrain dynamics. Wheel traces are visually rendered, but not physically simulated.

The **RSIM Lunar Surface Simulator** [9] (formerly known as the VIPER Lunar Surface Simulator [10]), developed by NASA's Ames Research Center and built on top of Gazebo, features many crucial aspects of lunar exploration. The simulator includes realistic lighting, camera lens flare and synthetically enhanced large-scale terrain. It consists of a slope-dependent wheel slip model, derived at the NASA Glenn SLOPE facility, which uses a 'slip map' to simulate loss of traction. However, this model does not consider velocity-dependent slip behavior, and wheel sinkage due to slip is not visually or physically represented. Wheel traces are rendered using bump mapping, which creates the illusion of deformation by altering surface normals; however, it does not modify the actual terrain mesh. The trace rendering does not consider wheel geometry or slip.

OmniLRS is an open-source lunar robotic simulator based on NVIDIA Omniverse IsaacSim and was developed by the University of Luxembourg and the Space Robotics Lab at Tohoku University [3]. It features three environments: (1) the Lunalab, a replica of the lunar testbed located at the University of Luxembourg, (2) the Lunaryard, a procedurally generated lunar terrain, and (3) a large-scale lunar environment based on lunar digital elevation maps. The simulator has demonstrated successful sim-to-real transfer in vision-based rock segmentation tasks using the Lunalab environment. Wheel traces are visually represented and scaled

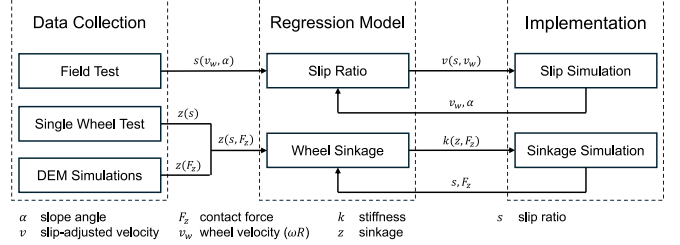


Fig. 2. Architecture of the proposed method.

through a contact-force-based regression model, which can be tuned to suit a grouser wheel if the mesh geometry of the wheel is available [11]. However, the simulator lacks full terramechanics considerations, such as a slip plugin or wheel sinkage visualization.

B. Terramechanics Simulators

Terramechanics simulators prioritize the accurate computation of interactions between vehicles and terrain over the realistic visual representation of synthetic environments. In addition, typically, rover perception and control are either simplified or lacking.

For high-fidelity modeling, the discrete element method (DEM), originating with the works of Cundall and Strack [12], can be used to model lunar soil as a collection of particles that interact with one another and a wheel of the vehicle traversing the terrain. Contact forces and torques are calculated using computationally intensive methods with high spatial and temporal resolution. DEM has been widely used in terramechanics to study slip, wheel sinkage and soil deformation. Coupling DEM with multi-body dynamics enables detailed analyses of planetary rover mobility on granular material, ranging from complex single-wheel motion and suspension systems to full rover studies [13]. However, the method is not suitable for real-time applications and lacks support for robotic control and sensors.

To address this limitation, frameworks such as Project Chrono [14] offer multiple deformable terrain models. While supporting DEM, Chrono has a continuous representation model (CRM) and a soil contact model (SCM). SCM computes contact forces between surfaces and the ground, allowing for terrain mesh deformation and contact response in near real-time. However, simulations are restricted to small environments and lack integration with robotics stacks for perception and control.

III. METHODOLOGY

This work aims to bridge high-fidelity terramechanics simulations and real-time photorealistic robotics environments using a data-driven approach, as illustrated in Fig. 2. Regression models for wheel slip and sinkage, derived from field tests, single-wheel experiments, and DEM simulations, are integrated into the lunar surface simulator OmniLRS [3]. Slip ratio s is simulated by commanding the rover to follow a slip-adjusted velocity v , while sinkage z is modeled via compliant contacts (spring-damper system), where stiffness

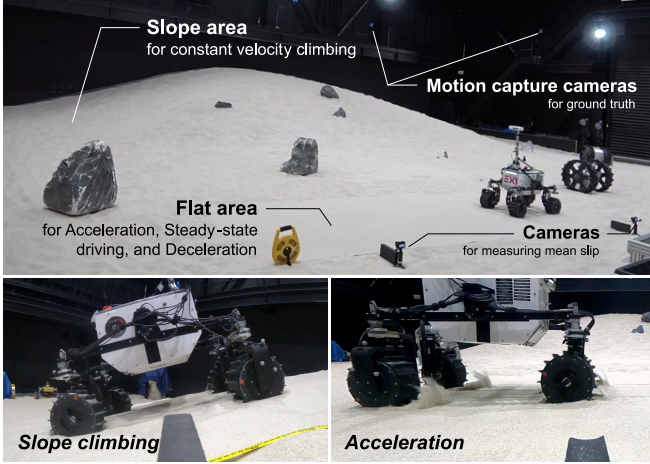


Fig. 3. Experimental setup of the data acquisition field test (top) and two representative snaps of slope climbing (bottom-left) and acceleration (bottom-right).

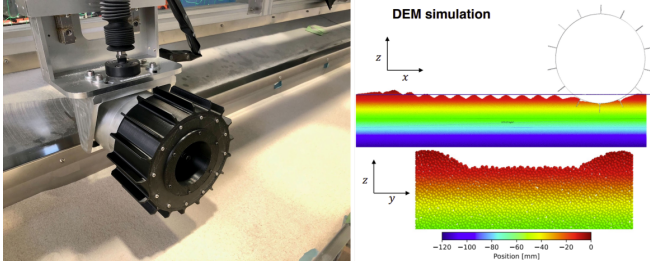


Fig. 4. Single wheel testbed (left) [15] and DEM simulation (right) [16].

k determines the sinkage depth. In addition, the contributions include improved terrain deformation for wheel trace rendering that not only scales with the contact force F_z , as implemented in [11], but additionally with the slip ratio s . This paper focuses on the implementation method rather than on data collection or regression modeling.

A. Experiment Procedure

To measure the wheel slip, field tests were conducted at the JAXA Space Exploration facility [2], using EX1, a four-wheeled high-speed rover of dimensions (0.82, 0.52, 0.67 m) and weighing 21.63 kg, equipped with a passive spring-damper suspension developed at the Space Robotics Lab [1]. The wheel design is optimized based on the grouser spacing equation in [17]. The data collection test was designed as shown in Fig. 3. The experimental site features a 20 m \times 20 m area filled with of Tohoku Silica No.5 [18] sand of about 0.3 m in depth. This dry loose silica sand is commonly used in terramechanics research as a low-fidelity lunar regolith simulant. Its sparse grain distribution presents even more challenging conditions for wheel sinkage and slippage [15].

Tests were performed on flat terrain across wheel velocities ($v_w = \omega R$) of 0.23 to 1.17 m/s, and on slopes ranging from 0° to 18° at speeds up to 0.47 m/s. Additional trials included rapid acceleration and deceleration to analyze transient slip (Fig. 3). Wheel speed v_w was measured via encoders, and translational velocity v was tracked using

a 16-camera OptiTrack motion capture system (180 Hz, ± 0.15 mm accuracy). To independently estimate average slip, external cameras recorded wheel rotation and traversal time over a defined 2 m section (also see Table I).

Slip ratio s was computed as shown in Equation 1, where ω is the angular velocity and R the effective wheel radius, including grouser height. In many studies of grousered wheel motion, only the wheel radius is used, ignoring grouser height for slip ratio calculations. However, it was found that if the grouser length were not included for slip calculations, then the slip would be calculated as negative or skidding during the driving motion. Including the grouser length as the effective wheel radius yields positive slip for all acceleration and steady-state motion. The slip or skid is then negative, as expected, during deceleration.

$$s = \begin{cases} 1 - \frac{v}{\omega R}, & \text{if } \omega R \geq v \\ \frac{\omega R}{v} - 1, & \text{if } \omega R < v \end{cases} \quad (1)$$

During acceleration and deceleration tests, the motion capture system also tracked vertical wheel displacement to estimate sinkage relative to the initial resting position. To complement the field data, prior results from single-wheel testbed experiments [15] and DEM simulations [16], [19] were referenced (Fig. 4), as DEM enables detailed analysis of wheel-soil interaction where physical testing is limited by controllability and measurement precision. The testbed provided slip-sinkage relationships, while DEM simulations at a fixed slip ratio of 20% were used to evaluate the influence of varied vertical loads.

B. Regression Models

Based on the experimental observations, regression models for wheel slip and sinkage were derived to characterize terrain interactions. The slip ratio s on flat terrain was found to increase linearly with wheel speed v_w , as expressed in Equation 2. The effect of slope angle α on slip ratio was captured by fitting a second-order polynomial with coefficients parameterized by v_w , resulting in the combined slip model shown in Equation 3. The polynomial fits were based on the averaged values from 16 independent experimental runs.

$$s(v_w) = 0.0265 v_w + 0.0256 \quad (2)$$

$$s(v_w, \alpha) = (0.00522 v_w + 0.00105) \alpha^2 + s(v_w) \quad (3)$$

The sinkage model was developed by combining results from the single-wheel testbed and discrete element method (DEM) simulations. Sinkage z was modeled as a linear function of slip ratio s and the deviation of vertical load F_z from a nominal reference load F_{ref} , which corresponds to the static load on a single wheel under uniform force distribution in lunar gravity. Static sinkage was measured by the motion capture system during the field tests. The sinkage regression model, where z is expressed in millimeters (mm), is given by:

$$z(s, F_z) = -33.56 s - 0.9291(F_z - F_{ref}) - 3.11 \quad (4)$$

TABLE I

OVERVIEW OF SENSORS, DATA, SAMPLING FREQUENCY, AND NUMBER OF DATA POINTS COLLECTED FOR SLIP RATIO AND SINKAGE ESTIMATION

Sensors	Recorded Data	Computed Data	Frequency	Data Points
Motion Capture System	Position $[x, y, z]$ and Orientation $[q_x, q_y, q_z, q_w]$	Velocity v	180Hz	≤ 1000
Cameras	Images	Avg. Velocity v	60Hz	-
Motor Encoders	Angular velocity $[\omega]$	-	5Hz	≤ 35



Fig. 5. Rover illustrated with visual wheel geometry (left) and physics wheel geometry (right).

C. Slip Implementation

In both real-world operation and high-fidelity terramechanics simulations, slip arises from complex interactions between the wheels and deformable terrain. In contrast, the present approach determines wheel slip using a regression model. At each simulation time step, the slip ratio s is computed by evaluating the regression model with the current wheel velocity v_w and local slope angle α as inputs. This slip ratio is then used to determine the slip-adjusted translational velocity v , defined as:

$$v = (1 - s(v_w, \alpha)) v_w \quad (5)$$

Since the simulation is based on rigid-body dynamics with Coulomb friction, it cannot reproduce steady-state slip, i.e., slip occurring during motion with a constant velocity. To replicate the kinematic effect of slip, the wheels are directly actuated with the slip-adjusted velocity v . This approach enables the realistic simulation of slip behavior while maintaining a rigid-body framework.

To reproduce the visual appearance of slipping wheels, each wheel is separated into a purely visual body for rendering and a purely physical body for physics interactions. Both representations share the same location but are connected to the chassis via separate joints, allowing independent actuation. The physical wheel is driven at the slip-adjusted velocity v , while the visual wheel rotates at the commanded wheel velocity v_w . A visual impression of wheel slip is then created, without actual slip occurring between the physics geometry and the terrain. While the visual geometry utilizes a detailed mesh for realistic representation of the grouser wheel, the physics geometry is based on a simple capsule (Fig. 5) to achieve stable contact interactions.

In addition to steady-state slip behavior, the rover's transient dynamics during acceleration and deceleration are essential for consistency with experimental data. Accordingly,

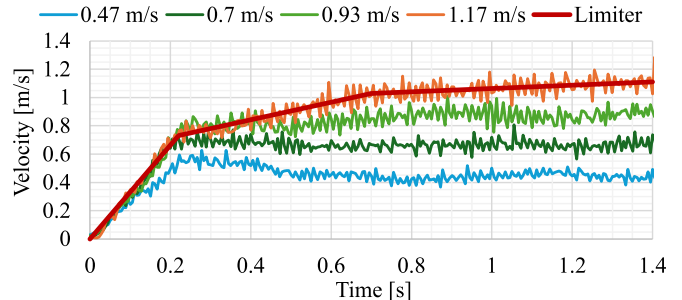


Fig. 6. Measured translational velocity during acceleration for four different commanded wheel velocities. The red curve represents the limiter function, which defines the maximum possible acceleration.

the simulation Coulomb friction model was calibrated using velocity profiles obtained from field tests. These tests showed that the rate of deceleration remained consistent from 0.2 m/s to 1.17 m/s for commanded velocities during rapid stops. By setting the static and dynamic friction coefficients to 1.0 and 0.8, respectively, the simulated deceleration closely matched the observed behavior.

However, the high friction parameters lead to unrealistically rapid acceleration. To address this, we introduced a limiter function that constrains the maximum allowable change in translational velocity between time steps. This constraint is based on field test data, where initial acceleration was largely independent of the commanded wheel velocity, indicating that it is limited by grouser geometry and soil characteristics. The field test data and the limiter are shown in Fig. 6. Notably, acceleration decreased beyond a certain velocity threshold, a trend that can be approximated using a piecewise linear function, defined as follows:

$$\Delta v \leq \begin{cases} 3.476, & \text{if } v \leq 0.75 \\ 0.612, & \text{if } 0.75 < v \leq 1.02 \\ 0.114, & \text{if } v > 1.02 \end{cases} \quad (6)$$

D. Sinkage Implementation

To model wheel sinkage on deformable terrain using only rigid bodies, we use compliant contact modeling. Rather than treating contacts as perfectly rigid, a spring-damper system simulates the vertical contact force between colliding bodies, the terrain and the wheels. The system is expressed as:

$$\ddot{z}(t) = -g - \frac{k}{m}z(t) - \frac{c}{m}\dot{z}(t) \quad \text{for } z(t) < 0 \quad (7)$$

Here, $z(t)$ is the penetration depth, $\dot{z}(t)$ the relative normal velocity, and $\ddot{z}(t)$ the relative acceleration of the two bodies. The parameters k and c are the stiffness and

damping coefficients, respectively, m is the effective mass at the contact, and g is gravitational acceleration. The vertical reference contact force is $F_z = mg$.

In quasi-static conditions (i.e., $\dot{z}(t) = \ddot{z}(t) = 0$), the penetration depth can be obtained by:

$$z = -\frac{F_z}{k} \quad (8)$$

Thus, for a vertical force F_z , the penetration depth z can be controlled by adjusting the stiffness k . Since our regression model provides the expected sinkage $z(s, F_z)$ as a function of slip ratio s and vertical load F_z , we invert the relation to determine the appropriate stiffness.

For grouser wheels, sinkage is typically measured relative to the base radius r , not considering sinkage of the grousers. When simulating grouser wheels using a physics geometry with radius $R = r+h$, the grouser height h must be explicitly considered in the equation to achieve the correct sinkage.

Collisions between the wheels and the terrain may be resolved at a single or multiple contact points, with the total load distributed among these points. To achieve the correct penetration depth z , the stiffness k must be scaled by the number of contact points N , as shown in Equation 9. It is advisable to use simple physics geometries for rover wheels, such as spheres or capsules, that produce steady contact forces through a consistent number of contact points.

$$k = -\frac{1}{N} \frac{F_z}{z(s, F_z) - h} \quad (9)$$

For numerical stability, minimum thresholds are enforced for both the contact force F_z and the denominator in the stiffness calculation. This prevents divisions by zero and avoids near-zero stiffness values that could otherwise lead to unstable behavior when F_z is small.

The stiffness parameter k is updated at each timestep based on the current contact force and slip ratio, which can lead to unrealistic behavior during deceleration. As the rover skids, high slip causes deep sinkage. Once it stops and slip drops to zero, the recalculated sinkage becomes shallower, causing a sudden increase in k and making the rover rise visibly. To avoid this artifact, sinkage is constrained when the translational velocity v falls below $v_{min} = 0.1$ m/s:

$$z^{(t)} \leftarrow \min(z^{(t-1)}, z^{(t)}), \quad \text{if } v^{(t)} \leq v_{min} \quad (10)$$

Complementing the stiffness parameter, the damping constant d affects the dynamic response of the contact. In this work, the damping constant is set to critical damping (Equation 11), which ensures stable behavior:

$$c = 2\sqrt{km} \quad (11)$$

E. Terrain Deformation

The terrain implementation by Kamohara et al. [11] is extended by incorporating slip, in addition to contact forces, as a second parameter influencing the shape and depth of wheel traces. Higher slip values result in deeper terrain deformation, and the amplitude of the sinusoidal trace pattern left behind by grouser wheels is reduced under high slip

conditions, which is consistent with field test observations. In addition to the geometric adjustment of the wheel, the deformation mechanism was separated into two components: permanent depth deformation and transient trace patterns. This separation enhances the visual fidelity of overlapping wheel traces, particularly when the rover traverses the same area multiple times.

In the current version, depth deformation is only updated if the newly computed depth d is greater (i.e., deeper) than the existing value at a given terrain cell $d_{x,y}$. In contrast, the trace pattern w is regenerated and applied on every pass, allowing for realistic wheel trace visuals. The combination of depth d and trace w results in realistic and dynamic terrain modifications in the digital elevation map. The update logic is defined as:

$$\begin{aligned} \Delta d &\leftarrow \min(0, d - d_{x,y}) \\ \Delta w &\leftarrow w - w_{x,y} \\ DEM_{x,y} &\leftarrow DEM_{x,y} + \Delta d + \Delta w \\ d_{x,y} &\leftarrow d_{x,y} + \Delta d \\ w_{x,y} &\leftarrow w \end{aligned}$$

F. Simulation Setup

The implementation was developed using the robotics simulator IsaacSim (version 2023.1.1) in combination with the OmniLRS environment. The slip and sinkage models were implemented as Omnidigraphs, primarily utilizing custom script nodes. The wheel trace functionality was directly integrated into the OmniLRS base code. All simulations were performed in the Lunaryard environment with default physics settings [3] and a simulation timestep of 30 Hz.

IV. RESULTS AND ANALYSIS

The implementation was evaluated by comparing simulation results for slip ratio and wheel sinkage against the outputs of the regression models, providing a measure of how accurately the simulation reproduces expected behavior.

On flat terrain, the slip ratio error remained below 0.02% across all wheel speeds up to 1.17 m/s on flat terrain. For inclined terrain with slope angles up to 20°, the mean absolute error averaged to 0.22%. The average error in sinkage depth was 0.25 mm across the full range of slip ratios and contact force variations within ± 5 N of the reference force of 8.72 N under lunar gravity.

Additionally, Fig. 7 directly compares the simulation to the field test results on flat terrain for a commanded wheel velocity of $v_w = 1.17$ m/s, showing close agreement during steady-state motion, acceleration, and deceleration. The top graph shows v_w and the measured translational velocities v . The middle graph compares slip ratios, and the bottom plots display sinkage depth relative to the start of acceleration (left) and deceleration (right).

Fig. 8 shows a top-down view of wheel traces generated using the improved terrain deformation model. Highlighted areas indicate deformation depths exceeding 12 mm: blue and red mark regions of high slip during acceleration and

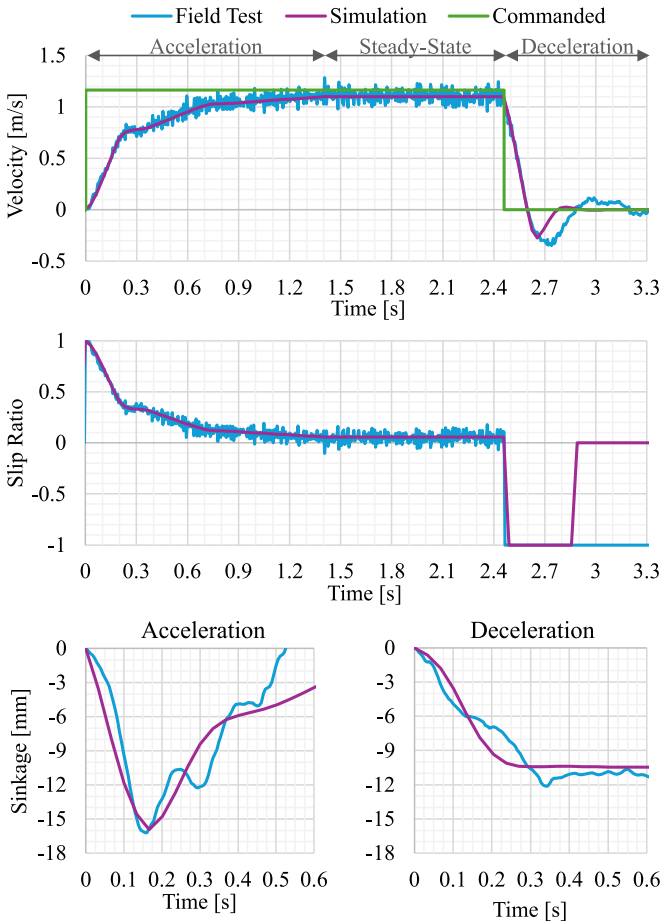


Fig. 7. Comparison between results from field test and simulation for the same experiment at a commanded wheel velocity of 1.17 m/s, including sudden acceleration and deceleration phases.

deceleration, while white corresponds to turning-induced deformation from increased load on the outer front wheel.

Finally, our simulator operates as shown in Fig. 9, achieving realistic wheel slippage and sinkage, as well as physical deformation of the terrain mesh, i.e., wheel traces on the lunar surface.

The proposed method accurately reproduced slip and sinkage behavior, confirming the effectiveness of using a regression-based terramechanics model. Although tuned for a specific rover-terrain combination, it is compatible with other configurations by substituting the regression model with one derived from new experimental data.

While slip was considered at various velocities, on upward and downward slopes, and during acceleration and deceleration on flat terrain, side slip and wheel-dependent slip during turns were not explicitly addressed. Furthermore, the current regression models are based on dry silica sand, which exhibits different and more uniform mechanical properties than lunar regolith. Developing regression models using actual lunar regolith simulants or in-situ lunar data, potentially with online adaptation methods, represents an important direction for future work to improve applicability to real missions.

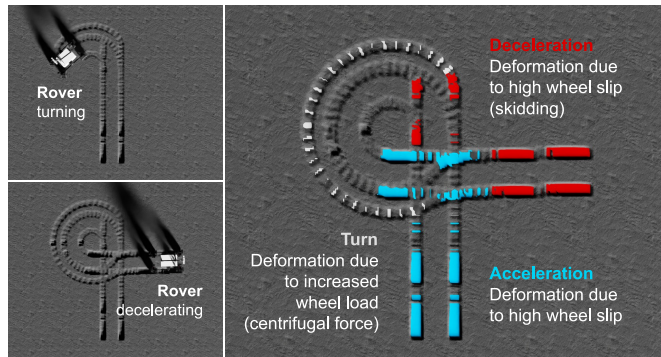


Fig. 8. Visible terrain deformation after rover traversal, with highlighted areas indicating locations where deformation depth is greater than 12 mm.

V. CONCLUSIONS

This work presented a data-driven approach to replicating realistic rover traversal on lunar terrain in real-time simulations. By integrating a regression-based terramechanics model, the implementation accurately captured both steady-state and dynamic slip and sinkage behavior, showing strong agreement with field test results. It also improved the realism of terrain deformation and wheel track visualization.

The method supports real-time applications where physically realistic terrain interaction responses are important, such as mobility analysis, rover testing, mission planning, or digital twin environments. Future work should focus on adapting to legged robot surface interaction to enhance simulation fidelity across diverse platforms used in space robotics.

ACKNOWLEDGEMENT

The authors would like to thank Simon Giel, Momoko Shimizu, Antoine Jonquieres, Takeaki Komine, Yoshimasa Muneishi and Nette Levijoki for their invaluable support in field testing and data collection.

REFERENCES

- [1] D. Rodríguez-Martínez *et al.*, “Enabling faster locomotion of planetary rovers with a mechanically-hybrid suspension,” *IEEE Robotics and Automation Letters*, pp. 1–8, 11 2023.
- [2] JAXA. (Accessed: 2024-12-09). [Online]. Available: <https://www.ihub-tansa.jaxa.jp/english/>
- [3] A. Richard *et al.*, “OmniLRS: A photorealistic simulator for lunar robotics,” in 2024 *IEEE International Conference on Robotics and Automation (ICRA)*, vol. 21, May 2024, p. 16901–16907.
- [4] NVIDIA IsaacSim. (Accessed: 2025-03-09). [Online]. Available: <https://docs.isaacsim.omniverse.nvidia.com/latest/index.html>
- [5] E. Z. Crues *et al.*, “Digital Lunar Exploration Sites (DLES),” in 2022 *IEEE Aerospace Conference (AERO)*, 2022, pp. 1–13.
- [6] C. Foreman *et al.*, “Digital Lunar Exploration Sites (DLES) Terrain Crafting,” in 2025 *IEEE Aerospace Conference*, 2025, pp. 1–18.
- [7] R. Vondrák *et al.*, “Lunar Reconnaissance Orbiter (LRO): Observations for Lunar Exploration and Science,” *Space Science Reviews*, vol. 150, no. 1-4, pp. 7–22, February 2010. [Online]. Available: <https://doi.org/10.1007/s11214-010-9631-5>
- [8] L. Bingham *et al.*, “Digital Lunar Exploration Sites Unreal Simulation Tool (DUST),” in 2023 *IEEE Aerospace Conference*, 2023, pp. 1–12.

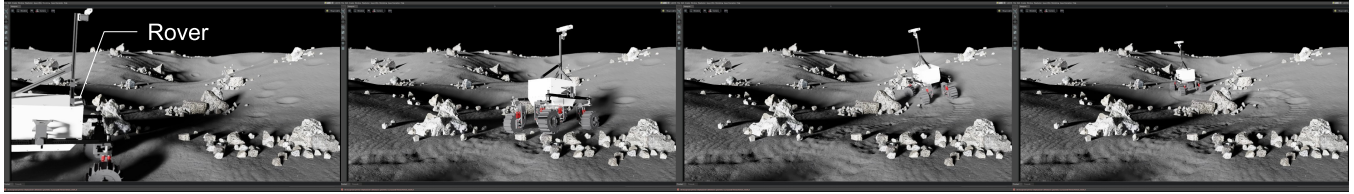


Fig. 9. Snapshots of our completed simulation platform, showing the four-wheeled EX1 rover traversing the digital lunar environment. Wheel slip and sinkage change dynamically with the terrain (slope angle) and the rover's motion (wheel velocity, contact forces) according to the regression models. Wheel traces are visualized through real-time deformation of the visual terrain mesh. When traversing rocks, the very high compliant contact stiffness assigned to them effectively prevents any wheel sinkage.

- [9] M. Allan, "RSIM Lunar Surface Simulator," Presentation at the Digital Twins for Cislunar & Lunar Surface Enterprise Integration Workshop #3, NASA Ames Research Center, Moffett Field, CA, United States, Apr. 2025, public Use Permitted. NASA Technical Review by Peer Committee. Contract: 80ARC020D0010. [Online]. Available: <https://ntrs.nasa.gov/citations/20250004026>
- [10] M. Allan *et al.*, "Planetary rover simulation for lunar exploration missions," in *2019 IEEE Aerospace Conference*, 2019, pp. 1–19.
- [11] J. Kamohara *et al.*, "Modeling of terrain deformation by a grouser wheel for lunar rover simulator," in *21st International and 12th Asia-Pacific Regional Conference of the International Society for Terrain-Vehicle Systems (ISTVS)*, 01 2024.
- [12] P. A. Cundall and O. D. L. Strack, "A discrete numerical model for granular assemblies," *Géotechnique*, vol. 29, no. 1, pp. 47–65, 03 1979.
- [13] T. M. Wasfy *et al.*, "Coupled Multibody Dynamics and Discrete Element Modeling of Vehicle Mobility on Cohesive Granular Terrains," in *10th International Conference on Multibody Systems, Nonlinear Dynamics, and Control, ASME*, vol. 6, 08 2014, p. V006T10A050.
- [14] A. Tasora *et al.*, "Chrono: An Open Source Multi-physics Dynamics Engine," in *International Conference on High Performance Computing in Science and Engineering*, 06 2016, pp. 19–49.
- [15] K. Takehana *et al.*, "Grouser wheel high-speed traction performance: DEM simulation and experimental result," *Journal of Terramechanics*, vol. 120, p. 101084, 2025.
- [16] J. Hurrell *et al.*, "Traction performance evaluation for a rashid-1 rover wheel," *Space Science Reviews*, vol. 221, no. 3, p. 37, 2025.
- [17] K. Skonieczny *et al.*, "A grouser spacing equation for determining appropriate geometry of planetary rover wheels," in *Proceedings of the IEEE/RSJ International Conference on Intelligent Robots and Systems (IROS)*, Vilamoura-Algarve, Portugal, Oct. 2012, pp. 5065–5070.
- [18] Tohoku Keisa Sangyo Co., Ltd., "Tohoku silica sand no.5," <https://www.ktsangyo.co.jp/data1.htm>, 2024, accessed: 2025-06-25.
- [19] J. Hurrell *et al.*, "Lunar rover discrete element method study and calibration," in *Proceedings of the 16th European-African Regional Conference of the ISTVS (ISTVS '23)*, Lublin, Poland, 2023.